Journal of Solid State Chemistry 185 (2012) 56–61

Contents lists available at SciVerse ScienceDirect

Journal of Solid State Chemistry

journal homepage: www.elsevier.com/locate/jssc

Revisiting the properties of delafossite $CuCrO_2$: A single crystal study

Maria Poienar [a,b,*], Vincent Hardy [a], Bohdan Kundys [a], Kiran Singh [a], Antoine Maignan [a], Françoise Damay [c], Christine Martin [a]

[a] Laboratoire CRISMAT, UMR 6508 CNRS, ENSICAEN, 6 Bd. du Maréchal Juin, 14050 Caen Cedex, France
[b] National Institute for Research and Development in Electrochemistry and Condensed Matter, Plautius Andronescu Str Nr 1, 300224 Timisoara, Romania
[c] Laboratoire Léon Brillouin, CEA-CNRS UMR12, CEA-Saclay, 91191 Gif-sur-Yvette Cedex, France

ARTICLE INFO

Article history:
Received 26 August 2011
Received in revised form
19 October 2011
Accepted 29 October 2011
Available online 7 November 2011

Keywords:
Delafossite
Morphology
Magnetic properties
Electric properties

ABSTRACT

Platelet-like single-crystals of delafossite $CuCrO_2$ have been successfully grown and characterised by X-ray diffraction and pole figures, scanning electron and atomic force microscopy. Transport measurements reveal that the resistivity is highly anisotropic, with a ratio of about 35 at 300 K between the in- and out-of-plane directions, reflecting the layered crystal structure. The magnetization and specific heat data show that $CuCrO_2$ undergoes a unique antiferromagnetic transition at $T_N=24.0$ K, in contrast to a recent report on $CuCrO_2$ single-crystals [16] showing the existence of two magnetic transitions, $T_{N1}=24.2$ K and $T_{N2}=23.6$ K, depending on the orientation of the applied magnetic field along and perpendicular to *c*, respectively.

1. Introduction

AMO_2 oxides (A=Cu, Ag, M=transition metal element) with the delafossite structure have attracted a lot of interest as prototype triangular lattice antiferromagnet (TLA) with a great number of interesting properties, as for instance negative thermal expansion [1–3], transparent conductivity [4,5] or mutiferroicity, like recently shown for $CuFeO_2$ and $CuCrO_2$ [6,7]. Owing to great technological and fundamental importance of multiferroic materials, new developments have been numerous in this field of research in the past years [8–10]. Among recently studied compounds, the $CuCrO_2$ delafossite (Cr^{3+}, $S=3/2$) is of prime interest, since, unlike $CuFeO_2$, it is ferroelectric, without application of a magnetic field or substitution upon the M-site. Ferroelectricity is induced in $CuCrO_2$ when it becomes antiferromagnetic (below $T_N=24$ K) with a noncollinear spin ordering [7] which is characterised by a helicoidal structure with an incommensurate propagation vector (q, q, 0), with $q \approx 0.329$ [11–13]. Neutron powder diffraction does not evidence any structural transition at T_N, though a small magneto-crystalline effect is noticeable [11]. Using high-resolution X-ray diffraction and strain gauge thermal expansion measurements on single crystal however, a small in-plane lattice distortion has been found at T_N [14], and suggested as a cause for the incommensurability of the spin structure [15]. Both studies [14,15] were performed on crystals grown from Bi_2O_3 flux, whose physical properties were first reported in Ref. [16]. Surprisingly, they did not correspond with those we have observed on $CuCrO_2$ crystals prepared by flux, following [17]. That is why we have revisited this compound, by growing and characterising carefully single crystals, as well for their structural and morphological properties as for the physical characterisations, i.e. magnetic, transport and dielectric measurements.

2. Materials and methods

Single crystals of $CuCrO_2$ were grown by the flux technique as previously described in Ref. [17]. This method is based on the thermal decomposition of $K_2Cr_2O_7$ (80 wt%) in the presence of CuO (20 wt%) at high temperature. 1 wt% of B_2O_3 was also added in order to increase both homogeneity of the solution and crystal growth. The mixture (30 g) was heated in air at 100 °C/h from room temperature up to 900 °C. After a 24 h plateau, the molten batch was cooled at a rate of 30 °C/h. The platinum crucible was then kept in boiling water for almost 24 h and the single crystals were extracted and cleaned in a Soxhlet water filtering installation. Black and shiny platelet-like crystals with typical size of $0.2 \times 0.1 \times 0.006$ cm^3 and mass of ≈ 10 mg were selected and analyzed. As anisotropy of the physical properties is an important issue, the single crystals were sorted out to ensure nearly regular shape and roughly constant thickness. Physical measurements were performed several times, and by using different samples, in

* Corresponding author at: CRISMAT UMR 6508, 6 Bd. du Maréchal Juin, 14050 Caen Cedex, France. Fax: +33 2 31 95 16 00.
E-mail address: maria_poienar@yahoo.com (M. Poienar).

0022-4596/$ - see front matter © 2011 Elsevier Inc. All rights reserved.
doi:10.1016/j.jssc.2011.10.047

order to ensure reproducibility and to confirm the intrinsic origin of the observed properties.

Crushed crystals were first characterized at room temperature by X-ray powder diffraction (XRPD) experiments carried out with a Panalytical Xpert Pro diffractometer (CuK_α, $12^\circ \le 2\theta \le 112^\circ$) equipped with an X'celerator detector. The crystalline quality and the orientation of the crystals were also checked by X-ray pole figure measurements, with a four circle Xpert MRD diffractometer using Cu–K_α radiation. The surface morphology of the crystals was imaged using scanning electron (Zeiss SUPRA 55) and atomic force (model Nanosurf) microscopes.

The magnetic properties were studied by collecting magnetization (M) data in both zero-field-cooling and field-cooling modes with a SQUID magnetometer (MPMS, Quantum Design, maximum magnetic field of 5 T) in a magnetic field of 0.3 T, from 5 to 290 K. The magnetization was measured along the direction of the applied external magnetic field, on crystals glued to a plastic straw using a small quantity of grease. Two geometries were used with the field either applied in the (a,b) plane (M_{ab}) or along c (M_c).

Heat-capacity measurements were carried out in zero field by means of a commercial physical properties measurements system (PPMS, Quantum Design) using a relaxation method with a 2τ fitting procedure.

For the resistivity (ρ) measurements using the four-probe technique, electrical contacts were made by depositing silver paste (Dupont 6838) with gold wires ($\varnothing = 25$ μm) to connect the crystal to the measurement set-up (PPMS, Quantum Design). The schematic representation of the two configurations used to measure both in-plane ρ_{ab} resistivity (the electric current applied perpendicularly to the c-axis) and out-of-plane resistivity ρ_c (the electric current applied parallel to the c-axis) will be presented in the plot of the results. This set-up allows only measurements with $R < 10^6\ \Omega$ to be made, so that ρ_{ab} and ρ_c measurements were only measurable in the range of 200–350 K.

Silver paste was used to make electrodes on single crystals surfaces for dielectric permittivity and polarization measurements. These measurements were carried out in a PPMS Quantum Design cryostat with the help of an Agilent 4248A RLC bridge and a Keithley 6517A electrometer. The isothermal magneto-dielectric effect was obtained by applying a magnetic field perpendicular to the direction of the AC electric field. The capacitance and dielectric loss were measured from 5 K to room temperature (rate 2 K min^{-1}) at different frequencies (5–100 kHz) to ensure that the transition temperature is not frequency dependent and the dielectric loss was always below 0.1%.

For the in-plane polarization, a poling electric field of +588 kV/m was applied at 40 K during cooling to align the electric dipoles in a given direction and then removed at 10 K. The stabilization of polarization was recorded (5 ks) before measuring the pyroelectric current. The pyroelectric current was recorded thereafter during heating at a rate of 5 K min^{-1}. Polarization was obtained by integrating this current with respect to time, the zero of polarization being chosen in the high temperature phase where the pyroelectric current is zero.

3. Results and discussion

As expected, the XRPD data (Fig. 1 (ii)) of the crushed crystals are characteristic of a single phase of the delafossite structure with the $R\bar{3}m$ space group and unit cell parameters $a = 2.9747(5)$ and $c = 17.1038(6)$ Å. Atomic arrangement corresponds to hexagonal compact oxygen double layers having octahedral sites occupied by the Cr^{3+} cations and linked through Cu^+ ions, which are themselves linearly coordinated to two oxygen ions (inset of Fig. 1). In Fig. 1(i), the presence of only the

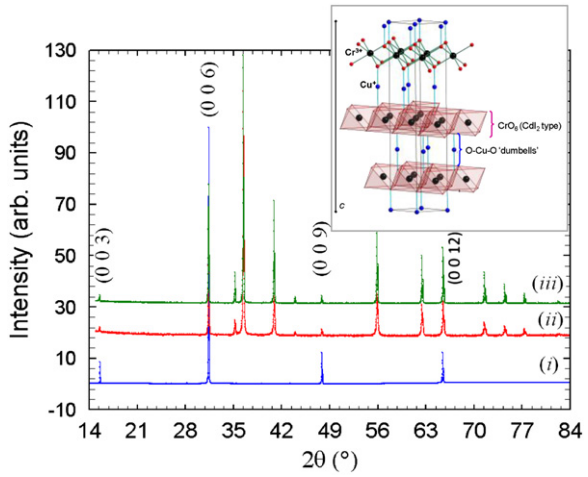

Fig. 1. (a) Room temperature X-Ray diffraction patterns for: (i) a plate-like single crystal were (0 0 l) reflections are shown (the c axis is perpendicular to the plane of the crystal); (ii) a crushed single crystal and (iii) polycrystalline sample. Inset: structure of $CuCrO_2$ delafossite (space group $R\bar{3}m$, $a = b = 2.9747(5)$ Å and $c = 17.1038(6)$ Å, hexagonal setting).

(0 0 l) reflections indicates that the c-axis is orientated perpendicularly to the plane of the crystal. This result confirmed also by X-ray pole figure measurements (not shown) indicates that the crystal is a single domain with rhombohedral symmetry and with the [0 0 1] direction perpendicular to the platelet.

Scanning electron microscopy (SEM) reveals clean surfaces, as shown in Fig. 2a. In the limit of the accuracy of the energy dispersive X-ray spectroscopy analysis, the actual cationic ratio corresponds to the nominal one (Cu/Cr ≈ 1). Nevertheless, some crystals exhibit defects in the shape of growth striations which form regular hexagons (of typical size about 80–100 μm) as shown in Fig. 2b. This kind of defect is characteristic of the flux method used for growing crystals; it evidences the instability of the growth interface [18]. The terraces forming the hexagon are perpendicular to the [0 0 1] direction and are descendent from the surface, creating holes. Atomic force microscopy images (Fig. 2c) reveal that the surface of some crystals exhibits rectilinear traces characteristic of a layer-by-layer growth, in agreement with SEM observations. Bubble inclusions are also visible, which can be related to evaporation at the surface, during the synthesis in air at high-temperature (900 °C). The size of these bubbles is influenced by the crystal growing steps and are smaller when they are included in the steps (Fig. 2c) [19].

A good agreement is observed between the magnetic susceptibility curves measured for single crystal (mass = 2.9 mg) and polycrystalline samples (considering the shape of the curves, the values of the magnetization and T_N). The temperature dependences of the magnetic susceptibilities (in-plane (χ_{ab}) and out-of-plane (χ_c)), plotted in Fig. 3, evidence a magnetic transition at $T = 24$ K, in agreement with the Néel temperature reported for polycrystalline $CuCrO_2$ [11,20]. Surprisingly, in the whole temperature range, there is only a slight difference between the $\chi_{ab}(T)$ and $\chi_c(T)$ curves, the latter being a bit lower than the former, below T_N. The $M(H)$ curves, collected at 5 K (not shown), are linear and similar in both configurations, a characteristic of strong antiferromagnetism. A similar $\chi_c \le \chi_{ab}$ relation was previously observed for the $CuCrO_2$ crystals prepared using a Bi_2O_3 flux [16], but in contrast, two T_N were reported for χ_c and χ_{ab}, at $T_{N1} = 24.2$ K and $T_{N2} = 23.6$ K, respectively. A close inspection of our single crystal data does not allow such an observation, the enlargement of the $\chi_c(T)$ and $\chi_{ab}(T)$ curves in the T_N vicinity is

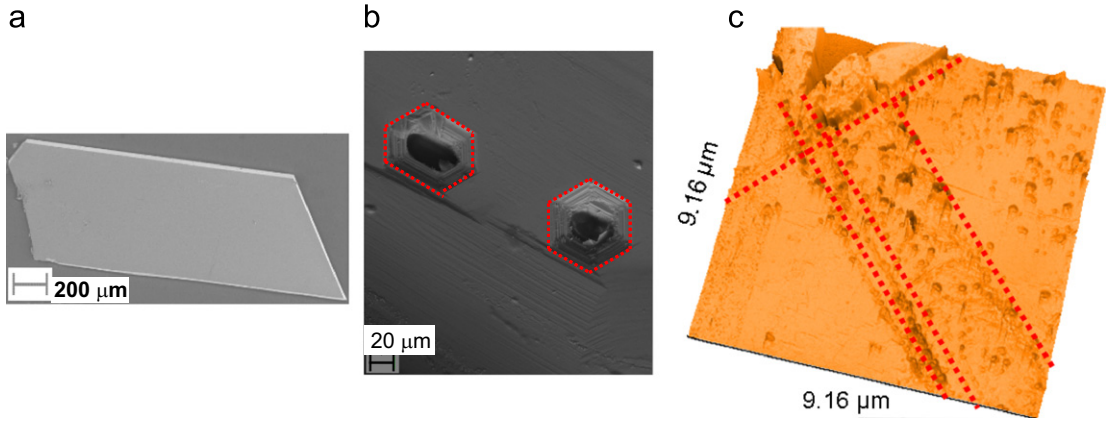

Fig. 2. (a) SEM image of a single crystal; (b) visualisation of some defects of the surface in the shape of regular hexagons (typical size of 80–100 μm); and (c) AFM image of a $CuCrO_2$ single crystal at $9.16 \times 9.16\ \mu m^2$. The red dash line is used to facilitate the visualisation of defects (in Fig. 2b) and dislocations (in Fig. 2c). (For interpretation of the references to colour in this figure legend, the reader is referred to the web version of this article.)

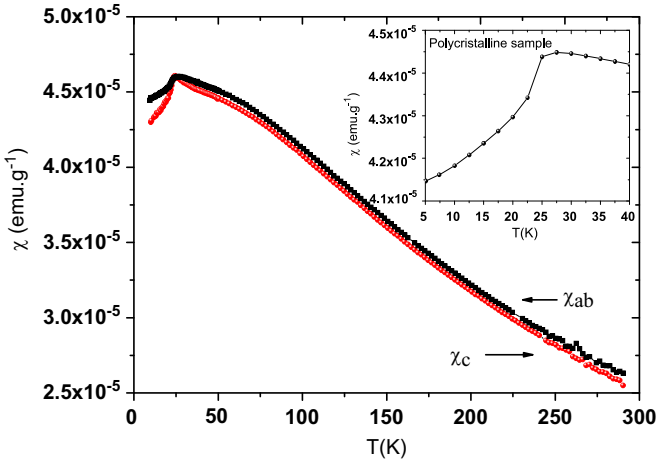

Fig. 3. Evolution with temperature of the susceptibility for a single crystal of $CuCrO_2$ in 0.3 T with the magnetic field applied in plane and out-of-plane (χ_{ab} and χ_c). Inset: susceptibility curve of a polycrystalline sample.

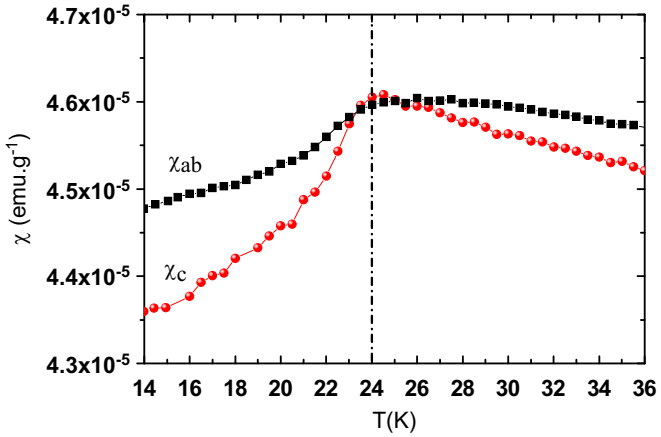

Fig. 4. Enlargement of $\chi_{ab}(T)$ and $\chi_c(T)$ in the vicinity of T_N ($\mu_0 H = 0.3$ T). The dashed line indicates the Néel temperature.

presented in Fig. 4, as it is in Ref. [16]. The unique T_N is corroborated by the specific heat (C) measurements versus temperature (mass = 12.9 mg) (Fig. 5a): only one transition is indeed observed on the $C(T)$ curve as well as in temperature derivative of the magnetic susceptibility (Fig. 5b). Here again, this result differs

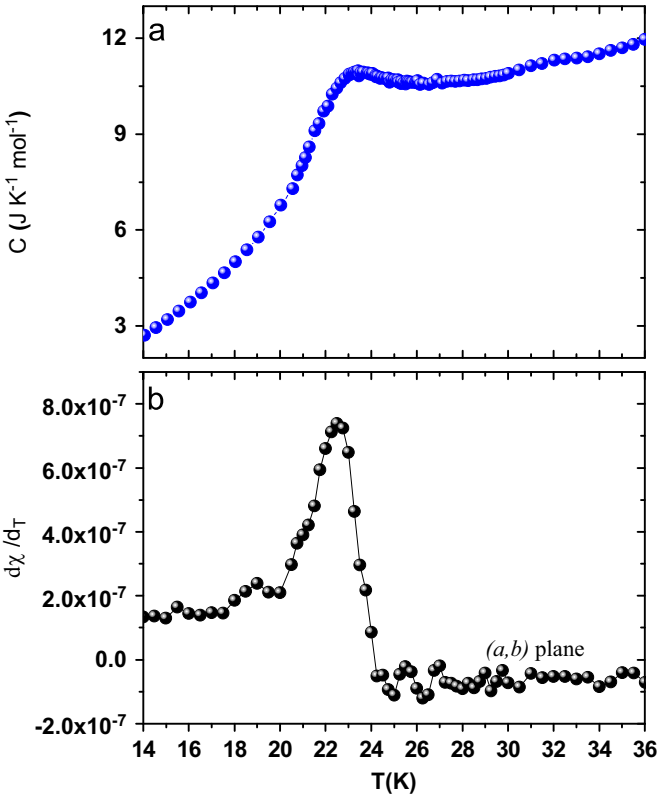

Fig. 5. (a) Variation with temperature of the specific heat in the vicinity of T_N ($\mu_0 H = 0$ T); and (b) temperature derivative of in-plane magnetic susceptibility ($\mu_0 H = 0.3$ T) for the $CuCrO_2$ single crystal.

from the one reported in Ref. [16] in which two T_N values were deduced from the double peak anomaly visible on the $C(T)$ curve.

The $\chi(T)$ and $C(T)$ curves of our crystals are comparable to those of polycrystalline samples, previously reported by several authors, with one transition observed in $\chi_{poly}(T)$ and $C_{poly}(T)$ curves [11,20,21]. In that respect, the reciprocal magnetic susceptibility curves, $\chi_{ab}^{-1}(T)$ and $\chi_c^{-1}(T)$, are also comparable to those of the polycrystalline samples. Above 150 K, a $\chi^{-1}(T)$ linear regime is evidenced for both crystal orientations. The Curie–Weiss fitting of the data of the single crystal leads to θ_{CW} values similar to the one obtained for a polycrystalline sample, that is, $\theta_{CW} = -194$ and -208 K, extracted from the $\chi_c^{-1}(T)$ and $\chi_{ab}^{-1}(T)$ curves, respectively, to be compared with -202 K for the

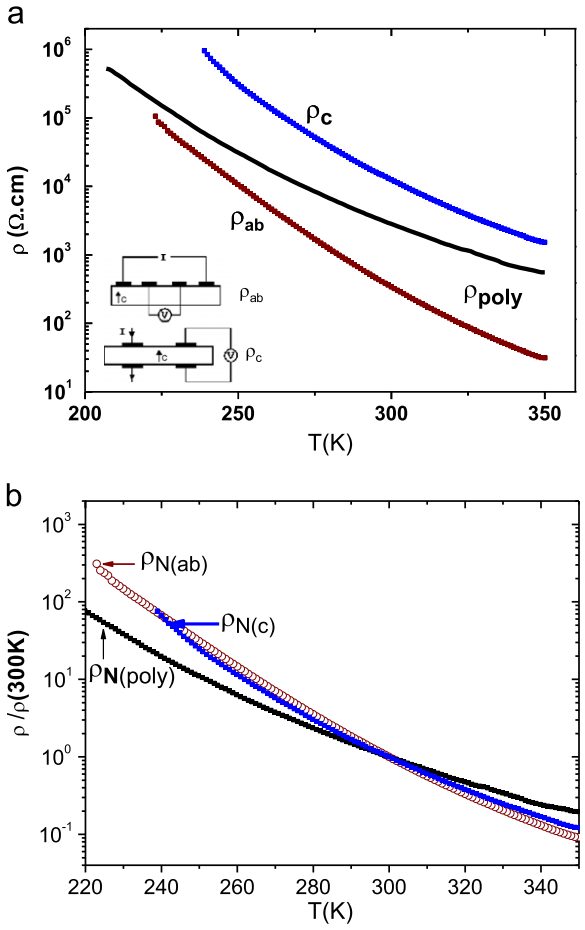

Fig. 6. (a) Temperature dependence of in- and out-of-plane resistivity for a single crystal and the resistivity measurement for polycrystalline sample, plotted for comparison. Inset: schematic representations for the measurement of electric anisotropy for single crystals: in-plane (ρ_{ab}) and out-of-plane (ρ_c) configurations; and (b) normalized curve at $T=300$ K for in- and out-of-plane measurements for a single crystal and for a polycrystalline one.

poly-crystal. The large ratio $|\theta_{CW}/T_N| \cong 8$, higher than that observed in conventional antiferromagnets, points towards magnetic frustration in that compound. Finally, the similarity between the $\chi_{ab}(T)$, $\chi_c(T)$ and $\chi_{poly}(T)$ curves demonstrates the lack of a strong magnetic anisotropy in $CuCrO_2$.

The resistivity $\rho_{ab}(T)$ and $\rho_c(T)$, measured upon cooling a $CuCrO_2$ crystal down from 350 K, are reported in Fig. 6a, along with the result obtained for a polycrystalline sample (ρ_{poly}). The corresponding normalized curves (Fig. 6b) show that, as T decreases, $\rho_{ab}/\rho_{ab(300\ K)}$ and $\rho_c/\rho_{c(300\ K)}$ increase much faster than $\rho_{poly}/\rho_{poly(300\ K)}$. This is also supported by the values of the activation energy, $E_a=280$ meV for the polycrystalline sample against $E_a \sim 436$ meV for the out-of-plane configuration and 409 meV for the in-plane configuration. The most important result coming out these resistivity measurements is the large value of the resistivity anisotropy, in marked contrast with the magnetic measurements. The in-plane resistivity ($\rho_{ab(300K)}=3.4\times10^2\ \Omega$ cm) is 35 times lower than the out-of-plane one ($\rho_{c(300\ K)}=1.25\times10^4\ \Omega$ cm). It shows that the [CrO_2] and/or [Cu^+] planes are better conducting pathways that the (Cr–O–Cu) one along c. Similar result, that is a high resistivity ratio, $\rho_{c}/\rho_{ab(300\ K)}=25$ ($\rho_{ab}^{300\ K}\sim1\times10^3\ \Omega$ cm and $\rho_c^{300\ K}\sim2.5\times10^4\ \Omega$ cm) has been reported for $CuAlO_2$ crystals [22]. In this compound, the conducting plane is the copper one, but the Cu^+–Cu^+ distance is shorter ($\cong 2.86$ Å) than in $CuCrO_2$ ($\cong 2.97$ Å). Nevertheless, according to electronic structure calculations performed for $CuCrO_2$, the d orbitals of Cr^{3+} are mainly contributed near the Fermi level as compared to those of Cu^+ [23]. This would imply that the carriers would be mainly in the Cr-based planes rather than in the Cu ones. Furthermore, the intermediate ρ_{poly} value of the polycrystalline sample, between ρ_c and ρ_{ab}, is characterized by a positive thermoelectric power. This strongly suggests that in the $CuCrO_2$ crystals the charge carriers are holes, as in $CuAlO_2$.

A promising issue for future device applications is the magneto-electric control achieved in the magnetically induced ferroelectrics [24–26]. This effect is also reported in delafossite $CuCrO_2$ in which the spin-chiral ferroelectric domains structure can be finely tuned using both magnetic and electric fields [16,27]. Therefore, to study the relationship between electric and magnetic orders in the $CuCrO_2$ single crystals under investigation here, dielectric measurements have been performed, without and with a magnetic field ($-9\ T \le \mu_0 H \le +9\ T$), applied perpendicularly to the AC electric current. The dielectric constant was measured in the (a,b) plane and along the c axis of the $CuCrO_2$ single crystals. There are two possible configurations for measuring the in-plane dielectric constant: c1 and c2, schematized in Fig. 7 inset. For the c1 configuration (Fig. 7), one peak is observed in the $\varepsilon(T)$ curve at $T_N=24$ K, whose position is frequency independent and for which losses are very low (not shown). For the second configuration (c2), ε' presents also a peak at T_N, at a maximal frequency of 100 kHz, but because of the shape and size of the measured single crystal, the electrodes are much smaller (and the capacitor thickness much larger) than in the c1 configuration, inducing very noisy measurements (not shown). For the measurement along the c-axis, a small anomaly is observed at T_N; the ε' value is multiplied by 2.9 in Fig. 8 to allow for a direct comparison with the result presented in Ref. [16] and the ε' value observed here is smaller than the one reported in Ref. [16].

The magneto-dielectric effect measured in the c1 configuration, at constant temperatures above and below the T_N, is presented in Fig. 9. The effect is symmetric under the application of ± 9 T, its magnitude increases with increasing temperature up to $T_N=24$ K and becomes zero at 25 K and its presents a hysteresis below T_N, more pronounced for $T=23$ K and which starts to develop at ~ 5 T (Fig. 9b). Hysteresis has been also observed in (dM/dH), ε and P vs. magnetic field curves of $CuCrO_2$ single crystals in [27] in which a magnetic transition occurs at $H_{flop}\sim 5.3$ T when the magnetic field is applied along the [1 -1 0]

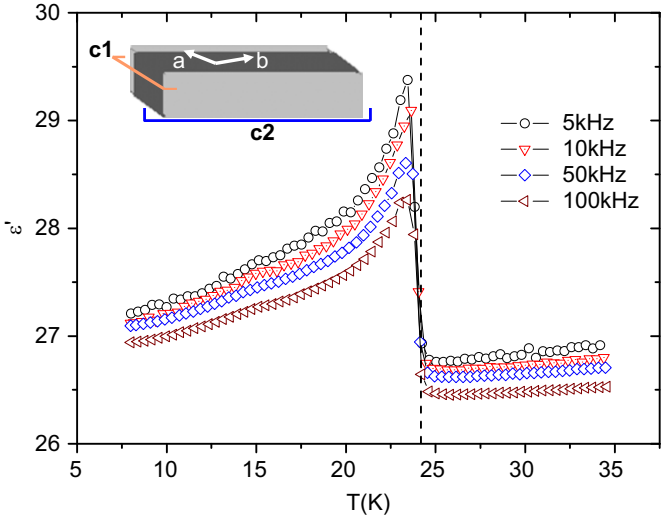

Fig. 7. Temperature dependence of the in-plane dielectric constant (at $f=5$, 10, 50 and 100 kHz) in the configuration c1 ($\mu_0 H=0$ T). Inset: schematic representation of the two possible configurations (c1 and c2) of electrodes on the single crystal surface for measuring the in-plane dielectric constant. The dashed line indicates the Néel temperature.

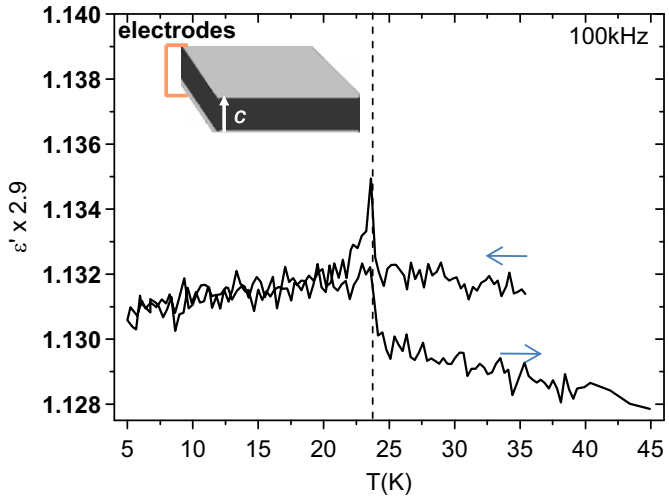

Fig. 8. Temperature dependence of the dielectric constant measured along *c* axis at 100 kHz (μ_0H=0T). Inset: the measurement configuration.

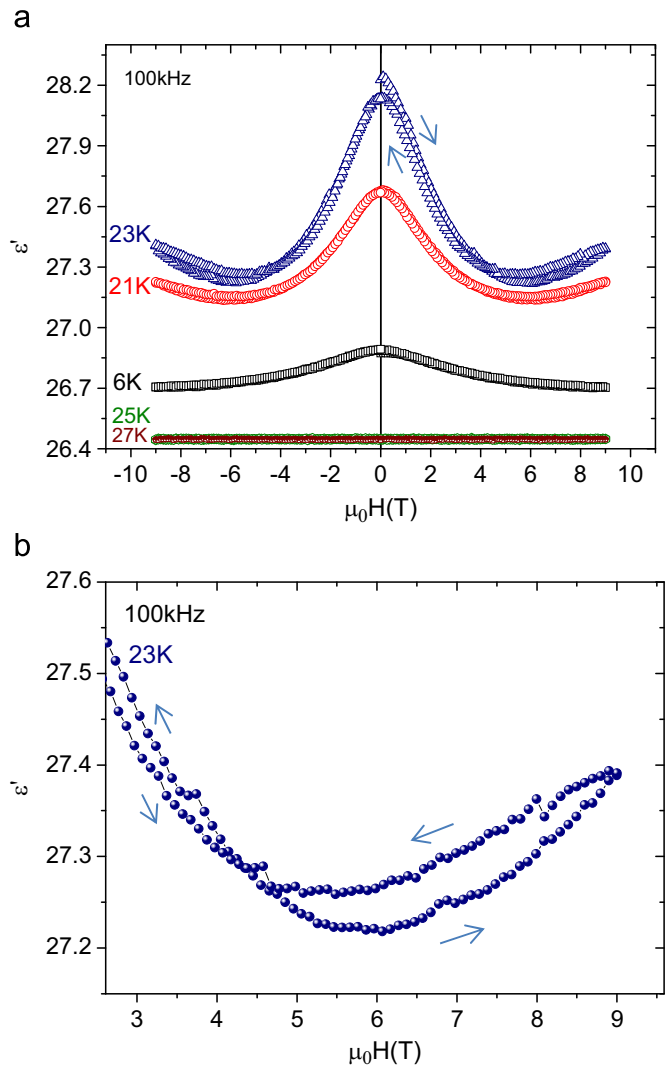

Fig. 9. (a) Magnetic field dependence of the dielectric constant (configuration c1) at constant temperatures (6, 21, 23, 25 and 27 K); and (b) enlargement between $\mu_0 H \sim 3$–9 T at $T=23$ K.

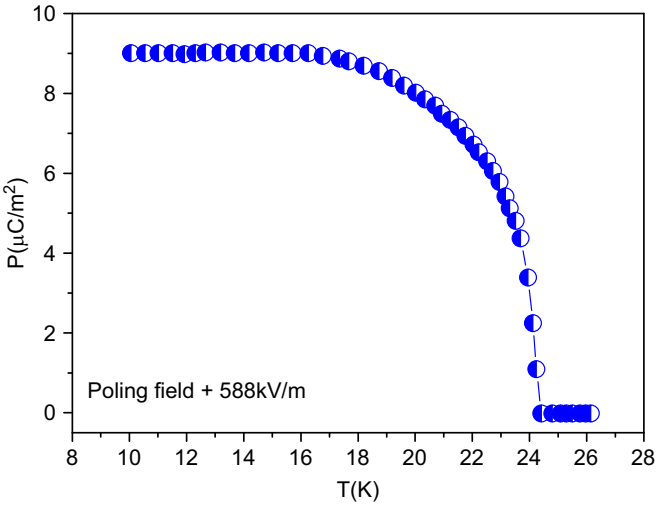

Fig. 10. Temperature dependence of the polarization in the (*a*,*b*) plane of the $CuCrO_2$ single crystal, obtained with a poling field of 588 kV/m.

direction, attributed to a transition from a proper-screw spiral to a cycloidal-spiral structure [28].

The polarization (P) in the (a,b) plane as a function of temperature crystal is shown in Fig. 10. As for the measurement on the polycrystalline sample [7,29], the polarization appears at $T_N=24$ K, confirming the spin ordering induced ferroelectricity. The polarization value is much smaller than that of the polycrystalline sample [7,29], and also than that reported in the literature for single crystals [16,27]; this could be related to the slightly different orientations of the electrodes compared to the single crystal crystallographic axes. In contrast, no polarization is measurable along the *c*-axis, a result of crucial importance, as it allows us to make a choice between the two magnetic structures, helicoidal or cycloidal, proposed initially in the neutron powder diffraction study [11]. The relation between the non-collinear magnetic order and the apparition of the polarization has been explained by symmetry considerations for the helicoidal structure (predicted along a) and by the 'spin-current' model for the cycloidal structure (predicted along c). The fact that the polarization is only measurable in the (a,b) plane of the single crystal, agrees with an helicoidal magnetic structure in $CuCrO_2$, as was also suggested by a recent inelastic neutron scattering study, in which spin wave calculations for an helicoidal structure model described the experimental data better than the cycloidal one [12].

4. Conclusion

Despite a rather isotropic magnetic behaviour, a large anisotropy is evidenced in the electric transport properties, with the resistivity ratio at 300 K, $\rho_c/\rho_{ab} \sim 35$. In contrast to a recent reports on $CuCrO_2$ single-crystals [16,30] showing the existence of a shift of the Néel transition depending on the relative orientation of the magnetic field and the crystal (24.2 K and 23.6 K), a unique antiferromagnetic transition is observed in the magnetization, as well as in specific heat curves, of our crystals, at $T_N=24.0$ K (likewise to polycrystalline samples). The discrepancies between the properties of single crystals prepared by flux method indicate that more efforts are necessary to characterize them with accuracy. In fact, it is well known that the physical properties of single crystals are highly dependent on the nature of the defects (twin boundaries, dislocations, impurity incorporation) as well as on their concentration [31–36]. To go further in the understanding of the spin-charge-lattice coupling in these

frustrated magnetic systems, it seems thus necessary to characterize carefully the structural, morphological and physical properties of delafossite single crystals prepared by several methods.

Acknowledgments

The authors thank L. Hervé, J. Aubril and J. M. Rueff for their technical assistance. The authors thank the French *Agence Nationale de la Recherche* for financial support (ANR-08-BLAN-0005-01).

References

[1] J. Li, A.W. Sleight, C.Y. Jones, B.H. Toby, J. Solid State Chem. 178 (2005) 285–294.
[2] J. Li, A. Yokochi, T.G. Amos, A.W. Sleight, Chem. Mater. 14 (2002) 2602–2606.
[3] S.I. Ahmed, G. Dalba, P. Fornasini, M. Vaccari, F. Rocca, A. Sanson, J. Li, A.W. Sleight, Phys. Rev. B 79 (2009) 104302.
[4] R. Nagarajan, A.D. Draeseke, A.W. Sleight, J. Tate, J. Appl. Phys. 89 (2001) 8022–8025.
[5] H. Kawazoe, M. Yasukawa, H. Hyodo, M. Kurita, H. Yanagi, H. Hosono, Nature 389 (1997) 939.
[6] T. Kimura, J.C. Lashley, A.P. Ramirez, Phys. Rev. B 73 (2006) 220401 (R).
[7] S. Seki, Y. Onose, Y. Tokura, Phys. Rev. Lett. 101 (2008) 067204.
[8] S.-W. Cheong, M. Mostovoy, Nat. Mater. 6 (2007) 13.
[9] J. van den Brink, D. Khomskii, J. Phys.: Condens. Matter 20 (2008) 434217.
[10] W. Eerenstein, N.D. Mathur, J.F. Scott, Nature 442 (2006) 759.
[11] M. Poienar, F. Damay, C. Martin, V. Hardy, A. Maignan, G. André, Phys. Rev. B 79 (2009) 014412.
[12] M. Poienar, F. Damay, C. Martin, J. Robert, S. Petit, Phys. Rev. B 81 (2010) 104411.
[13] M. Soda, K. Kimura, T. Kimura, M. Matsuura, K. Hirota, J. Phys. Soc. Jpn. 78 (2009) 124703.
[14] K. Kimura, T. Otani, H. Nakamura, Y. Wakabayashi, T. Kimura, J. Phys. Soc. Jpn. 78 (2009) 113710.
[15] H. Yamaguchi, S. Ohtomo, S. Kimura, M. Hagiwara, K. Kimura, T. Okuda, K. Kindo, Phys. Rev. B 81 (2010) 033104.
[16] K. Kimura, H. Nakamura, K. Ohgushi, T. Kimura, Phys. Rev. B 78 (2008) 140401(R).
[17] O. Crottaz, F. Kubel, H. Schmid, J. Solid State Chem. 122 (1996) 247.
[18] X. Li, J. Xu, H. Shen, A. Wu, X. Li, Phys. Status Solidi C 4 (2007) 1333–1336.
[19] X.H. Pan, W.Q. Jin, F. Ai, Y. Liu, Y. Hong, Cryst. Res. Technol. 42 (2) (2007) 133–137.
[20] J.P. Doumerc, A. Wichainchai, A. Ammar, M. Pouchard, P. Hagenmuller, Mater. Res. Bull. 21 (1986) 745.
[21] T. Okuda, Y. Beppu, Y. Fujii, T. Onoe, N. Terada, S. Miyasaka, Phys. Rev. B 77 (2008) 134423.
[22] M.S. Lee, T.Y. Kim, D. Kim, Appl. Phys. Lett. 79 (2001) 2028.
[23] A. Maignan, C. Martin, D. Pelloquin, E. Guilmeau, R. Frésard, V. Eyert, M. Poienar, Solid State Commun. 149 (2009) 962–967.
[24] N. Hur, S. Park, P.A. Sharma, J.S. Ahn, S. Guha, S.-W. Cheong, Nature 429 (2004) 392.
[25] T. Kimura, T. Goto, H. Shintani, K. Ishizaka, T. Arima, Y. Tokura, Nature (London) 426 (2003) 55.
[26] T. Kimura, Y. Tokura, J. Phys.: Condens. Matter 20 (2008) 434204.
[27] K. Kimura, H. Nakamura, S. Kimura, M. Hagiwara, T. Kimura, Phys. Rev. Lett. 103 (2009) 107201.
[28] M. Soda, K. Kimura, T. Kimura, K. Hirota, Phys. Rev. B 81 (2010) 100406(R).
[29] K. Singh, B. Kundys, M. Poienar, J. Charles Simon, J. Phys.: Condens. Matter 22 (2010) 445901.
[30] M. Frontzek, G. Ehlers, A. Podlesnyak, H. Cao, M. Matsuda, O. Zaharko, N. Aliouane, S. Barilo, S.V. Shiryaev, 2011. e-print 〈arXiv:1109.1747〉 [cond-mat.mtrl-sci].
[31] X.L. Wang, J. Horvat, H.K. Liu, J.N. Li, S.X. Dou, Phys. Rev. B 55 (1997) 3402(R).
[32] V.N. Timofeev, I.G. Gorlova, Physica C 309 (1998) 113–119.
[33] M. Oussena, P.A.J. de Groot, S.J. Porter, R. Gagnon, L. Taillefer, Phys. Rev. B 51 (1995) 1389.
[34] I. Monot-Laffez, M. Dominiczak, F. Giovannelli, A. Ruyter, J. Appl. Phys. 101 (2007) 053502.
[35] Ö. Özdemir, D.J. Dunlop, J. Geophys. Res. 102 (B9) (1997) 20211–20224.
[36] V.N. Dumachev, Tehnical Phys. Lett. 31 (2005) 247–248.